A Physical Approach to Reduce Nonspecific Adhesion in Molecular Recognition Atomic Force Microscopy

Oscar H. Willemsen,* Margot M. E. Snel,*# Laurens Kuipers,* Carl G. Figdor,*# Jan Greve,* and Bart G. De Grooth*

*Department of Applied Physics, Applied Optics Group, University of Twente, Enschede, and #Department of Tumor Immunology, University Hospital Nijmegen, Nijmegen, The Netherlands

ABSTRACT Atomic force microscopy is one of the few techniques that allow analysis of biological recognition processes at the single-molecule level. A major limitation of this approach is the nonspecific interaction between the force sensor and substrate. We have modeled the nonspecific interaction by looking at the interaction potential between a conical Si_3N_4 tip with a spherical end face and a mica surface in solution, using DLVO (Derjaguin, Landau, Verwey, Overbeek) theory and numerical calculations. Insertion of the tip-sample potential in a simulation of an approach-retract cycle of the cantilever gives the well-known force-distance curve. Simulating a force-distance curve at low salt concentration predicts a discrete hopping of the tip, caused by thermal fluctuations. This hopping behavior was observed experimentally and gave rise to a novel approach to making measurements in adhesion mode that essentially works in the repulsive regime. The distance between tip and sample will still be small enough to allow spacer-involved specific interactions, and the percentage of nonspecific interactions of the bare tip with the mica is minimized. We have validated this physical model by imaging intercellular adhesion molecule 1 (ICAM-1) antigen with a tip functionalized with anti-ICAM-1 antibody. The measurement demonstrated that a significant decrease in the number of nonspecific interactions was realized, and the topographical image quality and the specific bonding capability of the tip were not affected.

INTRODUCTION

The atomic force microscope (AFM) (Binnig et al., 1986) is able to image biological objects at nanometer resolution in aqueous solutions. The contact mode can reveal submolecular structures of crystallized proteins, but is too invasive to image individual molecules on a routine basis. The tapping mode in liquid (Hansma et al., 1994; Putman et al., 1994) circumvents this problem by oscillating a cantilever perpendicular to the sample, so that the lateral forces are minimized. The disadvantage of both modes, mentioned above, is that they only provide topographical information. All other surface properties mainly give rise to artifacts (van Noort et al., 1997; Müller and Engel, 1997). The most suitable mode in which to independently measure other surface properties like elasticity (Radmacher et al., 1994), electrostatic repulsion, and adhesion (van der Werf et al., 1994) is the so-called force-distance mode AFM. In this mode a force-distance curve is generated for every pixel of the scan, and from this curve the physical parameters, mentioned above, are deduced. This information can then be used to simultaneously construct an adhesion and topographical image. A disadvantage of this mode is that it is relatively slow compared to tapping mode (van Noort et al., 1998), but previous studies (Willemsen et al., 1998) showed that pixel rates of 25 Hz are attainable.

Received for publication 27 July 1998 and in final form 10 November 1998.

Address reprint requests to Dr. Bart G. de Grooth, Biophysical Techniques Group, University of Twente, P.O. Box 217, 7500 AE Enschede, the Netherlands. Tel.: 31-53-489-3157; Fax: 31-53-489-1105; E-mail: b.g.degrooth@tn.utwente.nl.

0006-3495/99/02/716/09 $2.00

The force-distance curve came to be of special interest in biophysical studies when it was used to measure the recognition between biomolecular pairs. Florin (Florin et al., 1994) and Lee (Lee et al., 1994) first demonstrated quantized adhesion forces between biotin and avidin. Subsequently, various groups (Dammer et al., 1996; Hinterdorfer et al., 1996; Allen et al., 1997) demonstrated recognition events between individual antibody-antigen pairs.

So far, all studies are hampered by the lack of topographical information, a most powerful parameter in conventional AFM. To construct a topographical image in adhesion mode, a force-distance curve for every pixel of an image is required. Because one scan requires at least 100×100 pixels, and a tip should be loaded with only one active recognition molecule, there is a large probability that the tip will lose its molecular specificity during a single image. Previously we have modified our AFM tip in such a way that it allowed stable imaging of individual ICAM-1 molecules with single molecular resolution in both topography and adhesion (Willemsen et al., 1998). The modification of the tip was accomplished via a polyethylene glycol spacer (Haselgrübler et al., 1995; Hinterdorfer et al., 1996), covalently coupling an antibody to the tip and providing flexibility to allow binding to the antigen on the substrate. Topographical and simultaneously recorded adhesion images demonstrated spatially resolved single-molecule recognition between anti-intercellular adhesion molecule 1 (anti-ICAM-1) antibody and ICAM-1 antigen. One of the limitations we faced was the nonspecific interaction between the bare silicon nitride tip and the mica substrate. Although we were able to distinguish between the specific and nonspecific interactions by the use of spacer technology

(Hinterdorfer et al., 1996), imaging the adhesion of the surface typically became more difficult after three consecutive scans (= 30,000 force curves). We observed an increasing affinity of the tip for the mica surface that coincided with a reduced quality of the adhesion image.

In the present study we have modeled the nonspecific interaction of the tip with mica with three terms: Born repulsion, van der Waals attraction, and electrostatic repulsion. We demonstrate that the new model qualitatively explains the observed force-distance curves and that the calculated adhesion force is in good agreement with experimental observations. Calculations of the interaction at low salt concentration gives further insight into the nonspecific adhesive bond formation. With the new information we were able to propose a novel approach that can decrease the number of nonspecific interactions: by imaging essentially in the repulsive regime, the probability of nonspecific adhesion can be minimized.

MATERIALS AND METHODS

A home-built AFM (van der Werf et al., 1993) was modified for sensitive force-distance measurements (Willemsen et al., 1998). All force experiments were carried out with silicon nitride cantilevers (Microlevers, cantilever B; Park Scientific Instruments, Sunnyvale, CA). The spring constant of the cantilever for the simulation was taken from the data sheet, and the cantilever of the recognition experiment was calibrated, using the thermal noise method (Hutter and Bechhoefer, 1993; Florin et al., 1995; Butt and Jaschke, 1995). The calculated value was 14 pN/nm, which is in reasonable agreement with the data sheet (20 pN/nm). To minimize drifts in our AFM that were caused by thermal gradients, all experiments were carried out in an airtight container. After the AFM was covered, it was allowed to thermalize for at least 20 min. All adhesion-mode images were taken at a pixel frequency of 25 Hz and contained 100 × 100 pixels. This resulted in a measurement time of 8 min/image. The cantilever was moved up and down with an amplitude of 90 nm.

Force-distance curves were recorded by sampling the deflection signal with 1000 points per approach-retract cycle. For the direct observation of thermal hopping, the AFM was left alone for an hour to thermalize. Thermal drifts in the *z* direction were now reduced to 4 nm/min. The tip displacement was measured by sampling the deflection signal at 2.5 kHz with a digital oscilloscope (Handyscope; TiePie Engineering, Sneek, The Netherlands) over a total measurement time of 400 ms. This means that the total drift in the *z* direction was 27 pm. The tip was brought within reach of the piezo tube (Stavely Sensors, East Hartford, CT) with a piezo spindle (Picomotor; New Focus, Santa Clara, CA) with an accuracy of 2 nm/step, after which the final approach was performed by putting a bias voltage on the tube.

Samples were prepared for the adhesion mode images in phosphate-buffered saline (PBS) (140 mM monovalent salt; Gibco, Life Technologies B.V., Breda, The Netherlands) by adsorbing ICAM-1 to freshly cleaved mica as described elsewhere (Willemsen et al., 1998). The thermal hopping experiment was carried out on freshly cleaved mica in a 3 mM KCl solution (pH 6). At this buffer concentration we verified the expected Debye decay length of 5.5 nm. This verification also gave us the force at zero distance F_0 (see Eq. 3) of 80 pN. Tips were functionalized with F10.2 antibody, which is directed against ICAM-1, using a 8-nm heterobifunctional PEG spacer, as described before (Haselgrübler et al., 1995; Hinterdorfer et al., 1996; Willemsen et al., 1998). The tip preparation procedure provided us with tips containing, on average, 0.7 active antibodies, which were used for specific recognition.

Conditions for the simulations

The simulation was based on the DLVO (Derjaguin, Landau, Verwey, Overbeek) theory (Israelachvili, 1991), applied to a spherical tip in the vicinity of a mica surface (Fig. 1 *a*). The total interaction energy between the two bodies is given by

$$U = \frac{H \cdot R}{3} \cdot \left(\frac{r_0^6}{7 \cdot D^7} - \frac{1}{2 \cdot D} \right) \quad (1)$$

in which H is the Hamaker constant for the silicon nitride-water-mica system (= 3.1×10^{-21}; Israelachvili, 1991), R is the tip radius, r_0 is used to include the Pauli exclusion force and is taken to be $1 \cdot 10^{-10}$ m (Rotsch

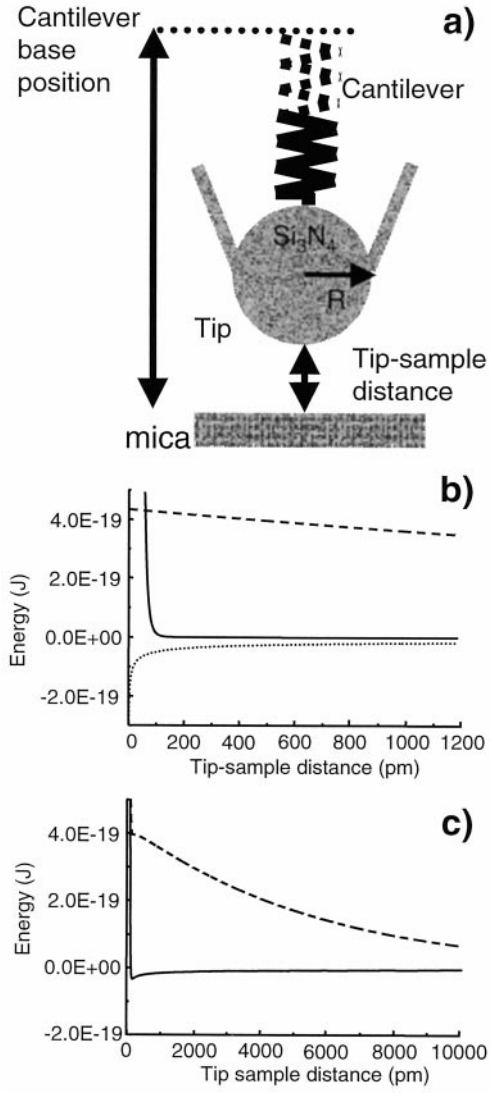

FIGURE 1 System for the calculation of force-distance curves. A conical tip with a spherical end face of silicon nitride is placed in the vicinity of a mica surface in aqueous solution (*a*). The salt concentration of the solution determines the amount of electrostatic energy. The tip is suspended from a cantilever that is modeled as a harmonic spring. The cantilever base position determines the rest position of the free cantilever. (*b*) Energy contributions to the tip-sample interaction potential. ——, Born repulsion; ·····, van der Waals attraction; – – –, electrostatic repulsion for 3 mM monovalent salt. (*c*) Tip-sample interaction potential with (– - –) and without (——) electrostatic repulsion.

and Radmacher, 1997), and D is the distance between the tip and the surface. The first term on the right-hand side of Eq. 1 is the repulsive term caused by the overlap between the electron orbitals of tip and mica (Born repulsion), and the second term is the van der Waals attraction. To account for the fact that the shape of the tip is not a sphere, but a cone with a spherical end face, we modified the long-range van der Waals attraction term. Butt (1991a) numerically calculated a van der Waals energy varying with $D^{-0.4}$ for a cone with a 90° top angle and a spherical end face with a radius of 10 nm. Therefore we replaced the second term of Eq. 1 accordingly to give

$$U = \frac{H \cdot R}{3} \cdot \left(\frac{r_0^6}{7 \cdot D^7} - 1 \cdot 10^6 \cdot \frac{1}{2 \cdot D^{0.4}} \right) \quad (2)$$

We used a tip radius (R) of 10 nm. The calculated values of the repulsive (*solid line*) and van der Waals contribution (*dotted line*) are shown in Fig. 1 *b*.

When the tip and mica are submersed in aqueous solution, the electrostatic energy U_{el} has to be taken into account. Butt (1991b) derived and experimentally verified the following relation:

$$U_{el} = F_0 \cdot \lambda_D \cdot e^{-D/\lambda_D} \quad (3)$$

where F_0 is the force at zero displacement and λ_D is the Debye decay length. In the equation it was taken into account that for the 3 mM KCl solution, both tip and sample become negatively charged and the decay is described by the full Debye length. The Debye length for monovalent salt at 22°C is given by (Israelachvili, 1991)

$$\lambda_D = \frac{0.304}{\sqrt{C}} \quad \text{(nm)} \quad (4)$$

in which C is the concentration of monovalent salt. For a 3 mM KCl solution we obtain a decay length of 5.5 nm. The electrostatic contribution is shown in Fig. 1 *b* (*dashed line*).

Both contributions, as described in Eq. 2 and plotted in Fig. 1 *b*, are added, and the result is plotted in Fig. 1 *c* (*solid line*). This curve shows the interaction potential between the tip without cantilever and the mica substrate. For the model calculations at low salt concentration we also need the electrostatic repulsion. Therefore we added the electrostatic contribution (Eq. 3) to the tip-sample interaction potential. The result is also shown in Fig. 1 *c* (*dashed line*).

The cantilever was modeled as a harmonic spring with potential energy U_{cant}:

$$U_{cant} = 0.5 \cdot k_{cant} \cdot x^2 \quad (5)$$

where k_{cant} is the spring constant of the cantilever (20 pN/nm) and x is the displacement from the equilibrium position (= deflection).

Software analysis of force-distance curves

An adhesion mode analysis package was written in Interactive Data Language (RSI). This package simultaneously displays a topographical image and concomitant adhesion image, and on every pixel the acquired force curve could be evaluated. Force curves were obtained by calibrating the deflection voltage in nanometers. For the calibration, the slope of a force curve, displaying a high nonspecific adhesion, was evaluated. The horizontal axis in a force curve is determined by the voltage on the calibrated piezo tube, so if the tip is in contact with the sample, the deflection has to follow the tube, giving a slope of 1. The deflection was multiplied by the spring constant to provide us with the correct forces.

Because adhesion events involving the spacer have a disruption behavior different from that of nonspecific interactions (Hinterdorfer et al., 1996, 1997; Willemsen et al., 1998), we can distinguish between both interactions by analysis of the force-distance curve. This is based on the fact that spacer-involved adhesions occur at tip-sample distances (rupture lengths) on the order of the spacer length. In contrast with this, nonspecific tip-sample adhesions occur at a rupture length of zero.

We have now written an algorithm that automatically classifies the observed interactions into three categories: no interaction (adhesion force smaller than 30 pN), spacer-involved interaction (rupture length larger than 3.5 nm), and nonspecific interaction.

RESULTS

Description of the model

The purpose of the present study is to find out whether we can minimize nonspecific interactions in molecular recognition experiments. To this end, we have created a physical model that describes the well-known force-distance curve.

Nonspecific adhesions between a silicon nitride tip and an infinite mica surface are usually depicted in force-distance curves. A force-distance curve is generated by moving the free cantilever toward the surface. First, the tip will snap into "adhesive" contact. Then it is pressed onto the surface until a preset maximum force, the so-called force set point, has been reached. Subsequently, the cantilever is retracted. Usually the curve is represented by plotting the deflection of the cantilever against the position of the cantilever base (see Fig. 1 *a*).

For simplicity we first simulated the force-distance curve without electrostatic repulsion and thermal fluctuations of the cantilever, so only the Born repulsion, van der Waals attraction (Eq. 2 and Fig. 1, *b* and *c*; see also Materials and Methods), and cantilever energy (Eq. 5) are considered. The location of the minimum in the cantilever potential depends on the position of the cantilever base (see Fig. 1 *a*). Moving the cantilever + tip toward the surface means a shift of the spring potential to the left in the energy plot. We have calculated the total energy of the system, mentioned above, for the equilibrium position of the free cantilever, located at 4.5, 3, 2, 1.3, and −2 nm. The total energy of the system at 4.5 nm is shown in Fig. 2 *a*. The total energy curve has only one minimum, located at 4.45 nm. The distance this minimum is shifted with respect to the original position of the undisturbed cantilever (*dashed line*) leads to a deflection of the cantilever. Because the shift is almost zero at this cantilever rest position, it is clear that the interaction of the surface with the tip is too weak to cause any deflection. In the second point of the simulation, the cantilever was moved 1.5 nm toward the surface. The total energy curve has been plotted as before in Fig. 2 *b*. The shift of the cantilever has now created two local minimums, i.e., two stable energy states. Because the simulation has been started with the free cantilever, the position of the tip is in the right well. The position of the minimum has been shifted with respect to the equilibrium position of the free cantilever, so the cantilever is deflected negatively. The third point of the simulation is generated by moving the cantilever 1 nm further toward the surface; the total energy curve is plotted in Fig. 2 *c*. It is clear that the deflection has increased, but that the tip is still in the right potential well. Now the cantilever is moved 0.7 nm further, and the energy curve is plotted in Fig. 2 *d*. The

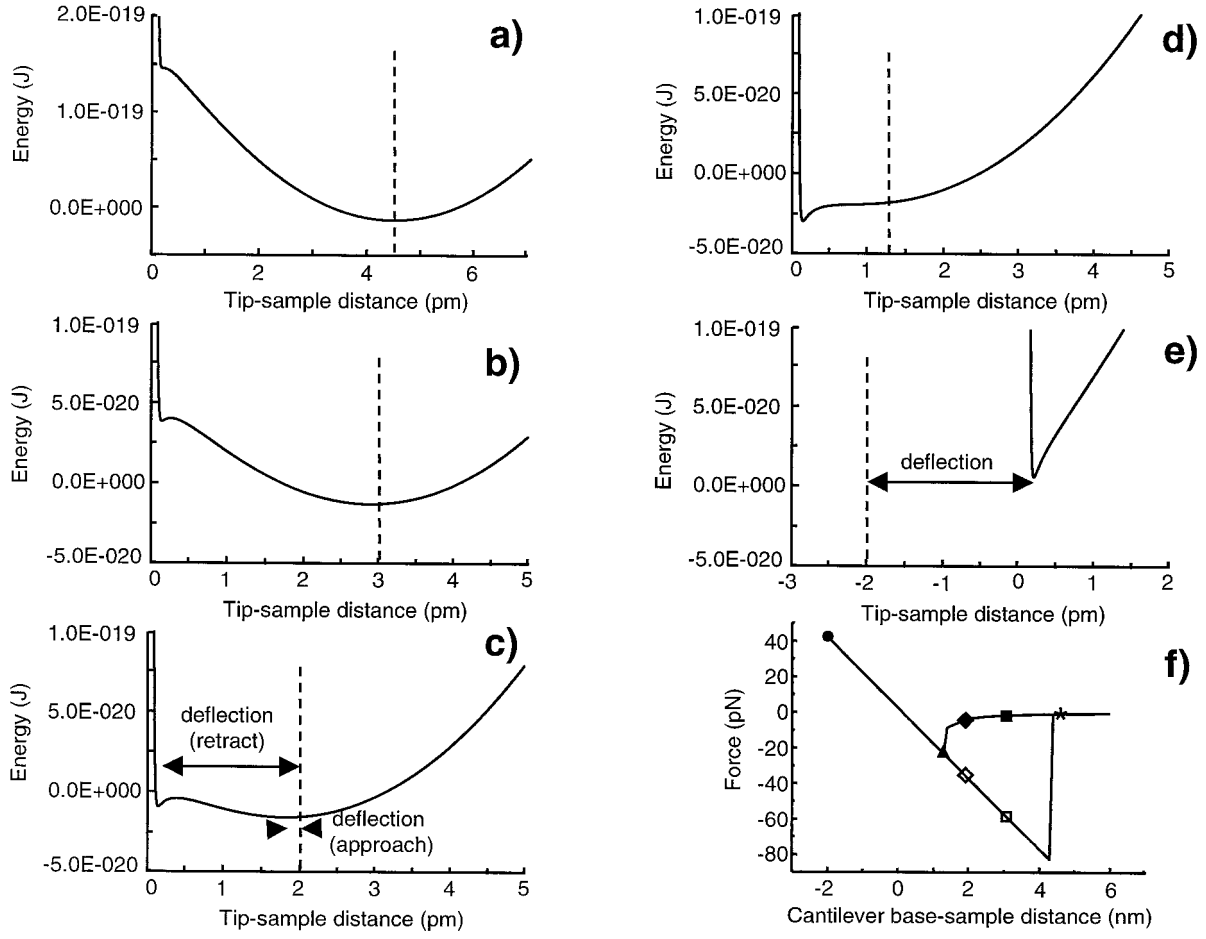

FIGURE 2 Total energy curves, consisting of the cantilever potential and the tip-sample interaction potential without electrostatic contribution. The base position of the cantilever is chosen such that the center position of the unperturbed cantilever (*dashed lines* in *a–e*) is located at 4.5 (*a*), 3 (*b*), 2 (*c*), 1.3 (*d*) and −2 nm (*e*). (*f*) Calculated force-distance curve. The calculated values from *a–e* are indicated by asterisks, squares, diamonds, triangles, and dots, respectively. Closed symbols are chosen for the approach and open symbols for the retraction of the tip + cantilever. For *a*, *d*, and *e* the symbols of approach and retraction overlap.

movement of the cantilever has resulted in a disappearance of the right potential, so suddenly the only stable state possible is located at 0.14 nm; the tip snaps into adhesive contact. If the cantilever is moved further toward the surface, the minimum of the total energy curve hardly shifts further, as shown in Fig. 2 *e*. In this case the deflection has become positive, so the tip is pressed onto the surface. When we now reverse the movement of the cantilever base, the tip remains in the left potential well. Moving the cantilever base from the surface apparently results in a deflection different from that resulting from moving toward the surface (see Fig. 2 *c*). This hysteresis in deflection is generally called the adhesion of the tip with the sample.

Using the above procedure, we calculated the deflection of the cantilever as a function of cantilever base position (Fig. 2 *f*). The points, corresponding to the situations in Fig. 2, *a–e*, are indicated by asterisks, squares, diamonds, triangles, and dots, respectively. The open symbols are used for the approach and the closed symbols for the retraction. We can now clearly recognize the familiar force-distance curve with snap into contact point, constant slope representing the spring constant, and the adhesion dip. The adhesion force for this typical tip sample configuration is 80 pN.

Adding electrostatic repulsion and thermal fluctuations: double well potential

Because all molecular recognition experiments are carried out in buffers with salt concentrations relevant to the molecules involved, we have to take into account the electrostatic repulsion. Therefore, we repeated the simulation for the same system, but now with the electrostatic repulsion for low (3 mM) and high (140 mM) salt concentrations. We now use the electrostatic interaction potential as described by Eqs. 3 and 4. The simulated force-distance curve at low salt concentration is shown in Fig. 3 *a*, and the curve at high salt concentration is shown in Fig. 4 *a*. We first focus on the curve with low salt concentration. The electrostatic repulsion causes the cantilever to deflect positively, before it

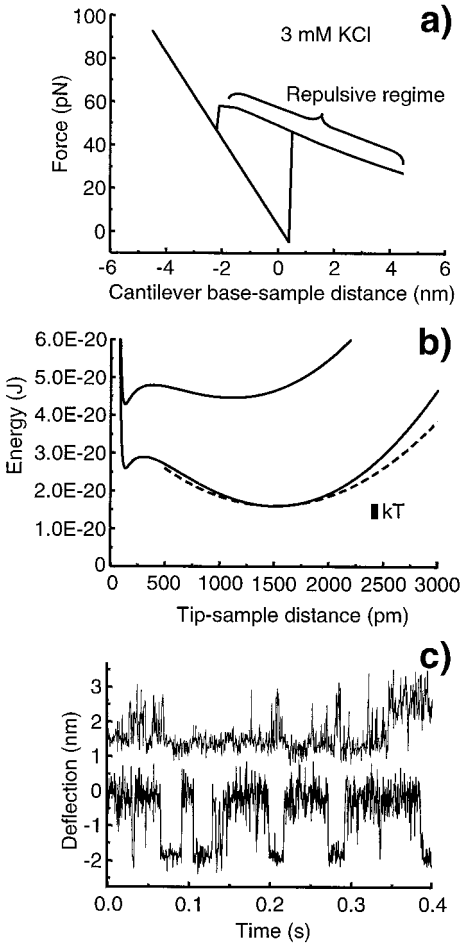

FIGURE 3 (*a*) Calculated force-distance curve that corresponds to the system of Fig. 1 *a*, submersed in 3 mM KCl. (*b*) Detailed view of the total energy curve when the rest position of the free cantilever is located at −1.3 (*lower curve*) and −1.8 nm (*upper curve*). Both curves show a double potential well with energy barriers on the order of 0.5*kT*, the thermal energy of a tip + cantilever. (*c*) Measured position of a tip in the vicinity of a mica surface. The upper trace corresponds to the upper curve of *b* and the lower trace to the lower curve of *b*. The spring constant of the right well is calculated from the lower trace. It is indicated by a dashed line in *b*. The upper trace has been raised by 3.3 nm for clarity.

snaps into adhesive contact. We call this region the repulsive regime. The snap into contact is somewhat smaller than in the situation without electrostatic repulsion, and clearly the adhesion dip is reduced to 50 pN.

When we consider the potential energy at −1.3 and −1.8 nm (= center position of the free cantilever potential), we have two energy curves that are plotted in Fig. 3 *b*. Both curves show a double well potential, with a separation of 1.0 and 1.5 nm, respectively. Although at a cantilever rest position of −1.3 nm the minimum on the right is energetically more favorable than the one on the left, the energy barrier to jumping to the left well is only 3*kT*, in which *k* is the Boltzmann constant and *T* is the temperature. When we take into account that the average kinetic energy of a tip + cantilever is 0.5*kT*, according to the equipartition theorem (Reif, 1965), it is likely that thermal fluctuations of the cantilever will induce a spontaneous jump to the left well. When the jump is made, it is highly unlikely to stay there, because in this well the energy barrier is only 1*kT*. This means that we expect to see a hopping behavior of the tip position, jumping back and forth between the two wells. When the cantilever base is moved toward the surface (see Fig. 3 *b*), the situation has changed; the probability of being in the left well increases at the expense of being in the right well. Thus we can expect a similar type of hopping behavior with an increased probability of being in adhesive contact (= the left well). Because the distance between the wells has decreased by 0.5 nm, the tip will make smaller jumps.

To test the prediction of this model, we have measured the tip displacement when it was brought close to the surface. A time trace was recorded and is plotted in Fig. 3 *c*. The lower trace represents the trace, which corresponds to the lower potential curve in Fig. 3 *b*. Indeed, we observed hopping behavior as predicted. The probability that the tip is located in the right well (= the state with high deflection) is indeed higher than the probability that it is in the left well. When the cantilever was moved toward the sample, the upper trace was recorded. The probability of being in the right well has clearly decreased. The distance the tip jumps has decreased by 0.5 nm, which shows that the cantilever has drifted for ~0.5 nm toward the mica. This observation demonstrates that by varying the distance between cantilever base and surface, we can modulate the probability of snapping into adhesive contact (in the left well).

Modulating the percentage of nonspecific interactions

The observation of thermal hopping suggests a novel approach to decreasing the number of nonspecific interactions. At the low salt concentration (3 mM) the interaction energy of tip and sample (Fig. 1 *c*, *dashed line*) has an energy barrier, which results in a repulsive regime in the force-distance curve. By setting the force set point sufficiently low that essentially we work in the repulsive regime (see Fig. 3 *a*), we could prevent the tip from snapping into adhesive contact. Thus in the energy curve of Fig. 3 *b* we remain in the right potential well. It should be noted however, that because of Brownian motion, there is always a chance that the tip will jump to the left well. The probability of a jump is strongly dependent on the force set-point value, as indicated by the previous experiment. Therefore the percentage of nonspecific adhesive contacts in an image is predicted to be dependent on the force set point used. At physiological salt concentration (140 mM), however, the repulsive regime is less pronounced (see Fig. 4 *a*). Already at very low repulsive forces (20–50 pN) the tip snaps into adhesive contact, and because in a typical adhesion mode experiment the set point is set at 100 pN at minimum, every force curve would result in an adhesive "hit." However, only if we use a very low force set point (±40 pN) do we expect to see the dependency on the force set point, as mentioned above. This was indeed observed in Fig. 4, *b* and *c*.

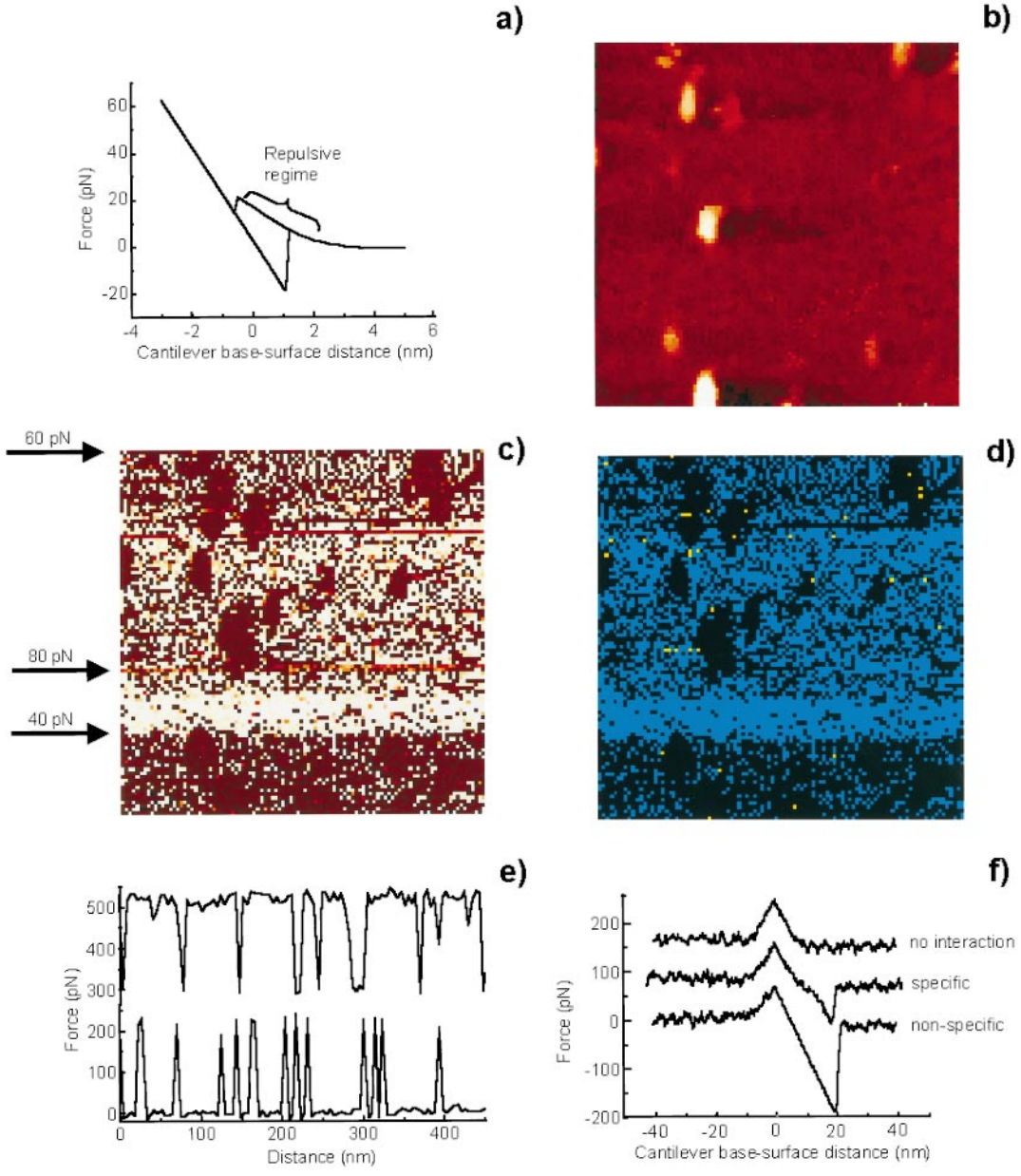

FIGURE 4 (*a*) Calculated force-distance curve that corresponds to the system of Fig. 1 *a*, submersed in 140 mM monovalent salt. (*b* and *c*) Simultaneously recorded topography (*b*) and adhesion image (*c*) of ICAM-1 molecules on a mica substrate. The images are acquired in adhesion-mode AFM with a tip that is functionalized with anti-ICAM-1 antibody via a spacer of 8 nm length. During the image scan the set point on maximum force is changed from 60 pN (line 1) to 80 pN (line 50) and from 80 to 40 pN (line 75). The image size is 420 × 420 nm. For the topography image (*b*) the height range is 0–9 nm. For the adhesion image (*c*) the force range is 0–300 pN. The height image is line-subtracted and median filtered by three pixels. (*d*) Adhesion image (*c*) after analysis of the force-distance curve taken on each pixel. Pixels, corresponding to curves without adhesion dips, are colored black, nonspecific interactions are colored blue, and specific interactions are colored yellow. (*e*) Line traces of *c* at a force set point of 80 (*upper trace*) and 40 pN (*lower trace*). The upper trace has been raised by 300 pN for clarity. (*f*) Three force-distance curves, selected from image *c*. The force curves are acquired on top of mica (*upper and lower curves*) and ICAM-1 antigen (*middle curve*) with a force set point of 60 pN. The approach distances are chosen negatively for separation of approach and retraction. The middle and upper curves have been raised by 75 and 150 pN, respectively.

Fig. 4, *b* and *c*, shows, respectively, the topographical and adhesion images of a sample of ICAM-1 adsorbed to mica. The topographical image shows individual ICAM-1 molecules lying on the flat mica background. During imaging of this surface in adhesion mode, the force set point on maximum force was changed. The image consists of 100 lines, and on line 50 the force set point was increased instantaneously from 60 to 80 pN. On line 75 it was decreased to 40 pN. Whereas variation in the force set point did not change the imaging capability, as shown in the topographical image (Fig. 4 *b*), the effect on the adhesion image is remarkable. When the force set point is raised, we see a substantial increase (25%) in the number of bright pixels, indicating that the probability of reaching adhesive contact has in-

creased. As expected, lowering the force set point decreases the percentage of high adhesion forces, even below the percentage at the beginning of the measurement (by a factor of 4). To show the magnitude of the adhesion force, the line traces at force set points of 80 and 40 are plotted in Fig. 4 *e*. At a high force set point, 85% of the times that a tip is brought near the mica surface, an adhesive contact is formed, resulting in a high adhesion force of ~250 pN. When the tip does not come into adhesive contact, it hardly shows any adhesion at all. This discrete behavior strongly supports the idea that there is either nonspecific adhesion or no adhesive contact at all. This observation is supported by the obtained force-distance curves. Fig. 4 *f* shows three adhesion curves, acquired with a force set point of 60 pN. The upper and lower curves were obtained on the mica substrate, and the middle curve was obtained on top of a molecule. The approach sections of the force-distance curves are shown with negative distances for clarity. The upper curve is a force curve that exhibits neither a detectable adhesion nor a snap into contact. In contrast to this, in the lower curve the tip has obviously snapped into contact, and retracting the cantilever and tip results in a nonspecific adhesion.

Although using a low force set point substantially reduces the number of nonspecific adhesive contacts, the distance between tip and sample (1–2 nm) is still small enough to allow specific bonding between anti-ICAM-1 antibodies and ICAM-1. Because of the spacers used to couple antibodies to the tips, we can bridge 8 nm (the spacer length is 8 nm). Indeed, the data of Fig. 4, *b–d*, were obtained with a tip functionalized with anti-ICAM-1 antibodies. By using the curve analysis method described in Materials and Methods, we can discriminate between nonspecific interactions of the bare tip and interactions involving the spacer molecules. In Fig. 4 *d* only the spacer-involved interactions are plotted in yellow, and nonspecific interactions are plotted in blue. The image shows that the specific interactions are mainly observed when the tip is located on an ICAM-1 molecule, whereas nonspecific interactions are exclusively observed when the bare tip is on the mica. An example of such a specific interaction curve is shown in Fig. 4 *f* (*middle curve*).

DISCUSSION AND CONCLUSIONS

We have modeled the interaction between a silicon nitride tip and a mica surface in solution, using DLVO theory, which was modified for a conical tip with a spherical end face of 10 nm (Butt, 1991a).

At physiological conditions the simulated force-distance curve of Fig. 4 *a* shows an adhesion dip of 30 pN, which corresponds perfectly to the experimentally observed adhesion forces of 20–50 pN for freshly prepared tips on mica. It should be noted that the force-distance curve was simulated without considering the thermal fluctuations of the cantilever. These fluctuations cause the tip to snap out of contact before maximum adhesion has been reached and therefore result in a smaller detected adhesion force. However, during a series of images (1 image = 10,000 force curves) we always observe an irreversible increase in these forces up to 250 pN. An increase in the van der Waals attraction is only possible if the tip is changed, but because we did not observe a change in the topographical image, we can rule out this reason. To find the reason for the increase, further investigation is required.

Model calculations using a low salt concentration resulted in the force-distance curve of Fig. 3 *a*. The most noticeable features are the repulsive regime before snapping into adhesive contact and the relatively small adhesion force. In this case the model predicts the occurrence of potential curves with double wells having barrier energies on the order of kT. Although the distance between the two wells is only ~1.5 nm, we were able to observe the thermal hopping between these energy states (Fig. 3 *c*). Both the distance between the "stable" positions and the probability of being either in the left or the right well show the predicted dependency of the distance between sample and cantilever base (Fig. 3, *b* and *c*). Furthermore, the thermal fluctuations in the right well are higher than those in the left well. The increase in the fluctuations is expected, because the right well is broader than the left well (see Fig. 3 *b*), and Brownian motion would thus result in different amplitudes for the two wells. From the observed fluctuations in the right potential well we calculated the effective harmonic potential. The result is shown in Fig. 3 *b* (*dashed line*), and it shows that the model is in good agreement with the experiment. The expected amplitude of the Brownian motion in the left well (0.1 nm) is smaller than the sensitivity of our beam deflection system (limited by the beam pointing stability of the laser diode).

A similar discrete hopping of the tip in the vicinity of a sample has been reported earlier by Cleveland and coworkers (Cleveland et al., 1995), who observed a triple potential well in the vicinity of a calcite surface. Hydration forces, which could be due to layering of solvent molecules, were responsible for the formation of the multiple potential wells. Because we used a low salt concentration, these hydration forces cannot be present in our case (Butt, 1991b).

The direct observation of the detailed tip movement in the vicinity of the surface allows one, in principle, to determine the complete potential curve, including all relevant parameters, such as activation energy, attempt frequency (Zangwill, 1988), and well distance.

Both modeling of the nonspecific interaction and experimental verification of the model by means of the observation of thermal hopping of the cantilever have led to the proposal of a new method to reduce nonspecific adhesion between tip and sample. We have shown that by using the repulsive force regime due to the electrostatic interaction at physiological salt concentration, we can minimize the probability of nonspecific adhesive contact (see Fig. 4 *c*). This concept has been used before to minimize tip-sample forces in the contact mode (Manne et al., 1994; Senden et al.,

1994). However, optimization of our AFM (electronics, stability, and force feedback; Willemsen et al., 1998) enabled us to operate essentially in the repulsive regime in adhesion mode. With this mode we have obtained high-resolution images of single ICAM-1 molecules. At the same time, the proposed method did not affect the ability of the functionalized tip to detect specific interactions (see Fig. 4 *d*) by the use of spacer technology (Hinterdorfer et al., 1996).

In principle it is possible to decrease the number of nonspecific interactions even more by lowering the force set point to 0 pN. In the adhesion mode we use, however, the cantilever is lowered toward the surface until the deflection has reached the force set point, after which the cantilever is retracted (see van der Werf et al., 1994, for details). Because the cantilever has force fluctuations of 20 pN, setting the set point lower than 40 pN would result in early retractions. Another solution is the use of a different cantilever. The cantilever spring constant acts on three parameters: the attempt frequency for hopping between energy states, the energy barrier to jumping into adhesive contact, and the minimum attainable value of the force set point. Because all of these parameters react in different ways, further simulations are necessary to determine the optimal spring constant.

Simultaneous imaging of topography in combination with software classification of the different kinds of adhesions (Fig. 4, *b–d*) shows that nonspecific interactions without the involvement of the spacer are observed exclusively on the mica. This causes the molecules to appear as black "holes" in the adhesion image (Fig. 4 *c*) that exactly follow the shape of the molecules in the topographical image. On the other hand, analysis of the spacer-involved adhesions (Fig. 4 *d*) shows that these interactions are mainly formed when the tip is on top of molecules. Because the antibody is attached to the tip by a spacer of only 8 nm length, the resolution of these specific adhesions is higher than that of the tip convolution-limited nonspecific interactions (Willemsen et al., 1998). From the line trace of the adhesion forces (Fig. 4 *e*) it is clear that the nonspecific adhesion has a discrete behavior; as predicted, either an adhesive contact has formed and retracting the cantilever from the surface results in an adhesion force of 250 pN, or no nonspecific bond is formed at all. It should be noted that the tip used showed higher nonspecific adhesion forces than freshly prepared tips. In contrast to this, the specific adhesion forces are ~100 pN, which is in good agreement with previous observations (Willemsen et al., 1998).

In conclusion, we can state that a detailed analysis of the nonspecific interaction between tip and substrate has led to a novel approach to reducing nonspecific interactions, and spacer-involved specific interactions can still be formed.

The authors thank H. Schindler, P. Hinterdorfer, and H. Gruber for kindly providing PEG spacers and P. Hinterdorfer for helpful discussion.

This research is supported by the Dutch Technology Foundation (STW).

REFERENCES

Allen, S., X. Chen, J. Davies, M. C. Davies, A. C. Dawkes, J. C. Edwards, C. J. Roberts, J. Sefton, S. J. B. Tendler, and P. M. Williams. 1997. Detection of antigen-antibody binding events with the atomic force microscope. *Biochemistry.* 36:7457–7463.

Binnig, G., C. F. Quate, and C. Gerber. 1986. Atomic force microscope. *Phys. Rev. Lett.* 56:930–933.

Butt, H.-J. 1991a. Electrostatic interaction in atomic force microscopy. *Biophys. J.* 60:777–785.

Butt, H.-J. 1991b. Measuring electrostatic, van der Waals, and hydration forces in electrolyte solutions with an atomic force microscope. *Biophys. J.* 60:1438–1444.

Butt, H.-J., and M. Jaschke. 1995. Calculation of thermal noise in atomic force microscopy. *Nanotechnology.* 6:1–7.

Cleveland, J. P., T. E. Schäffer, and P. K. Hansma. 1995. Probing oscillatory hydration potentials using thermal-mechanical noise in an atomic force microscope. *Phys. Rev. B.* 52:R8692–8695.

Dammer, U., M. Hegner, D. Anselmetti, P. Wagner, M. Dreier, W. Huber, and H.-J. Güntherodt. 1996. Specific antigen/antibody interactions measured by force microscopy. *Biophys. J.* 70:2437–2441.

Florin, E.-L., V. T. Moy, and H. E. Gaub. 1994. Adhesion forces between individual ligand-receptor pairs. *Science.* 264:415–417.

Florin, E.-L., M. Rief, H. Lehmann, M. Ludwig, C. Dornmair, V. T. Moy, and H. E. Gaub. 1995. Sensing specific molecular interactions with the atomic force microscope. *Biosens. Bioelectron.* 10:895–901.

Hansma, P. K., J. P. Cleveland, M. Radmacher, D. A. Walters, P. E. Hillner, M. Bezanilla, M. Fritz, D. Vie, H. G. Hansma, C. B. Prater, J. Massie, L. Fukunaga, J. Gurley, and V. Elings. 1994. Tapping mode atomic force microscopy in liquids. *Appl. Phys. Lett.* 64:1738–3740.

Haselgrübler, Th., A. Amerstorfer, H. Schindler, and H. J. Gruber. 1995. Synthesis and applications of a new poly(ethylene glycol) derivative for the crosslinking of amines with thiols. *Bioconjug. Chem.* 6:242–248.

Hinterdorfer, P., W. Baumgartner, H. J. Gruber, K. Schilcher, and H. Schindler. 1996. Detection and localization of individual antibody-antigen recognition events by atomic force microscopy. *Proc. Natl. Acad. Sci. USA.* 93:3477–3481.

Hinterdorfer, P., K. Schilcher, W. Baumgartner, H. J. Gruber, and H. Schindler. 1997. A mechanistic study of the dissociation of individual antibody-antigen pairs by atomic force microscopy. *Nanobiology.* 4:39–50.

Hutter, J. L., and J. Bechhoefer, 1993. Calibration of atomic-force microscope tips. *Rev. Sci. Instrum.* 64:1868–1873.

Israelachvili, J. N. 1991. Intermolecular and Surface Forces, 2nd Ed. Academic Press, London.

Lee, G. U., D. A. Kidwell, and R. J. Colton. 1994. Sensing discrete streptavidin-biotin interactions with atomic force microscopy. *Langmuir.* 10:354–357.

Manne, S., J. P. Cleveland, H. E. Gaub, G. D. Stucky, and P. K. Hansma. 1994. Direct visualization of surfactant hemicelles by force microscopy of the electrical double layer. *Langmuir.* 10:4409–4413.

Müller, D. J., and A. Engel. 1997. The height of biomolecules measured with the atomic force microscope depends on electrostatic interactions. *Biophys. J.* 73:1633–1644.

Putman, C. A. J., K. O. van der Werf, B. G. de Grooth, N. F. van Hulst, and J. Greve. 1994. Viscoelasticity of living cells allows high resolution imaging by tapping mode atomic force microscopy. *Biophys. J.* 67: 1749–1753.

Radmacher, M., J. P. Cleveland, M. Fritz, H. G. Hansma, and P. K. Hansma. 1994. Mapping interaction forces with the atomic force microscope. *Biophys. J.* 66:2159–2165.

Reif, F. 1965. Fundamentals of Statistical Thermal Physics. McGraw-Hill, New York.

Rotsch, C., and M. Radmacher. 1997. Mapping local electrostatic forces with the atomic force microscope. *Langmuir.* 13:2825–2832.

Senden, T. J., C. J. Drummond, and P. Kékicheff. 1994. Atomic force microscopy: imaging with electrical double layer interactions. *Langmuir.* 10:358–362.

van der Werf, K. O., C. A. J. Putman, B. G. de Grooth, and J. Greve. 1994. Adhesion force imaging in air and liquid by adhesion mode atomic force microscopy. *Appl. Phys. Lett.* 65:1195–1197.

van der Werf, K. O., C. A. J. Putman, B. G. de Grooth, F. B. Segerink, E. H. Schipper, N. F. van Hulst, and J. Greve. 1993. Compact stand-alone atomic force microscope. *Rev. Sci. Instrum.* 64:2892–2897.

van Noort, S. J. T., K. O. van der Werf, B. G. de Grooth, N. F. van Hulst, and J. Greve. 1997. Height anomalies in tapping mode atomic force microscopy in air caused by adhesion. *Ultramicroscopy.* 69:117–127.

van Noort, S. J. T., K. O. van der Werf, A. M. Eker, C. Wyman, B. G. de Grooth, N. F. van Hulst, and J. Greve. 1998. Direct visualization of dynamic protein-DNA interactions with a dedicated atomic force microscope. *Biophys. J.* 74:2840–2849.

Willemsen, O. H., M. M. E. Snel, B. G. de Grooth, J. Greve, P Hinterdorfer, H. J. Gruber, H. Schindler, Y. van Kooyk, and C. G. Figdor. 1998. Simultaneous height and adhesion imaging of antibody-antigen interactions by atomic force microscopy. *Biophys. J.* 75:2220–2228.

Zangwill, A. 1988. Physics at Surfaces. Cambridge University Press, Cambridge.